Nano Energy 31 (2017) 302–310

Contents lists available at ScienceDirect

Nano Energy

journal homepage: www.elsevier.com/locate/nanoen

An inductor-free auto-power-management design built-in triboelectric nanogenerators

Yunlong Zi[a,1], Hengyu Guo[a,b,1], Jie Wang[a,c,1], Zhen Wen[a], Shengming Li[a], Chenguo Hu[b], Zhong Lin Wang[a,c,*]

[a] School of Materials Science and Engineering, Georgia Institute of Technology, Atlanta, GA 30332, United States
[b] Department of Applied Physics, Chongqing University, Chongqing 400044, China
[c] Beijing Institute of Nanoenergy and Nanosystems, Chinese Academy of Sciences; National Center for Nanoscience and Technology (NCNST), Beijing 100083, China

ARTICLE INFO

Keywords:
Triboelectric nanogenerator
Power management
Energy harvesting
Self-powered system

ABSTRACT

Triboelectric nanogenerator (TENG) has the output characteristics of high voltage but low current/charge-transfer, making its low efficiency in powering most of electronics. To address this problem, power management circuits consisting of coupled inductors or transformers are usually employed. Here we report an inductor-free, auto-power-management design based on automatic switches between serial-connected and parallel-connected capacitors in a rationally designed manner, so that the output voltage can be lowered and the output charge is enhanced in proportion. In conjunction to theoretical analysis, a TENG along with proof-of-concept power-management units as automatically driven by the triggering motion for TENG is fabricated, which improves the rate for charging a supercapacitor by 5 times. Compared to previous work, this power-management design shows advantages of capability for harvesting low power/frequency scale energy, high scalability, and light weight, which paves a new approach for achieving high-efficient portable TENG-based self-powered system.

1. Introduction

With the rapid development of portable, wearable and implantable electronics, more and more attention has been dedicated to develop sustainable mobile power sources. Meanwhile, ambient mechanical energy associated to human motion provides an ideal power source for energy harvesting [1–4]. Among all of the mechanical energy harvesters, triboelectric nanogenerator (TENG) has attracted most of attention in recent years due to the advantages of high power output, high energy conversion efficiency, light weight, low cost, flexibility, scalability, and wide choice of materials [5–11]. However, as a capacitive-behavior energy harvester with high output impedance, TENG (typically with the size about 4 cm×4 cm) usually has a high voltage of typically hundreds of volts and low output current in ~μA level with charge transfer per half cycle of only ~0.1 μC. These characteristics result in low energy transfer efficiency for either powering electronics [12,13] or charging a battery [14,15] directly, since usually they have relatively low impedance. A proper power management strategy is required for TENG towards varieties of applications.

Traditional power management for energy harvesters especially TENGs is usually through a transformer based on electromagnetic induction effect. But in case of TENG, it leads to a huge power loss [13,16–18] because a transformer works the best at a designed frequency and bandwidth [12], which cannot be easily satisfied by TENGs that mainly harvest low-frequency energy with randomly-pulsed power [19]. Recently, Niu et al. have designed a power management system for TENG to operate mobile electronics sustainably [12]. However, the coupled inductors in this power management system still require a certain level of power (~100 μW level) from TENG for proper operation, and they also increase the total weight of the whole system and the difficulties for fabrication towards minimization. Previously, as an alternative strategy, switched capacitors have been used to regulate voltage and current outputs from thermoelectric and piezoelectric devices, as controlled by electronic switches [20–23]. However, this strategy for managing the low-frequency small-scale power output from TENG is still required to be studied; meanwhile, it is also worth to explore novel integration of automatic switches inside the TENG for utilizing the motion of the moving part to save energy consumed by electronic components, which cannot be achieved by most of other energy harvesters.

* Corresponding author at: School of Materials Science and Engineering, Georgia Institute of Technology, Atlanta, GA 30332, United States
E-mail address: zhong.wang@mse.gatech.edu (Z.L. Wang).
[1] These authors contributed equally to this work.

http://dx.doi.org/10.1016/j.nanoen.2016.11.025
Received 11 October 2016; Accepted 13 November 2016
Available online 22 November 2016

Here we report a power-management design based on switches between serial-connected and parallel-connected capacitors during the operation of TENG, so that the output voltage is lowered but the output charge is raised in proportion. A sliding freestanding-triboelectric-layer (SFT) mode [24,25] TENG was fabricated with the designed power-management unit as automatically triggered by the motion in TENG, using which a 5-time rate of charging a supercapacitor was demonstrated as compared with that through a rectifier directly. In practical, this power-management design is widely applicable for various TENGs with different power output levels and at any operation frequency especially the low power/frequency, with advantages of high scalability and light weight. This power-management design presents a novel route towards high-efficient portable TENG-based self-powered systems.

2. Results and discussions

2.1. Working principle of the power-management design

The operation of TENG is based on coupling of triboelectrification and electrostatic induction [6,7,26]. Initially, at least one pair of triboelectric layers with different materials are contacted to each other to create opposite triboelectric charges (Fig. S1a, Supplementary information, with an SFT mode TENG as an example). When the relative displacement between the triboelectric layers x changes from 0 to $x_{max,}$ the original electrostatic balance is broken and the potential difference between electrodes is built so that extra charges flow through external circuits to re-balance the electrostatic status (Fig. S1 b and c, Supplementary information). When the triboelectric layers move back from x=x_{max} to x=0, the charges flow in the reversed direction, returning to the original electrostatic status (Fig. S1 d and a, Supplementary information). Pulsed AC output possibly with random amplitude and variable frequency as dictated by external mechanical triggering is delivered to external circuits *via* the TENG. The major characteristic of the output is high voltage but low current/charge transfer, resulting in a low energy transfer efficiency for powering electronics with relatively low impedance. As for a general TENG, several important parameters are defined in Table 1, which are all consistent with that in previous studies [14,26].

The function of a power management unit for TENG is to improve the current output and lower the voltage with minimized energy loss, so that the output impedance can be decreased. As shown in Fig. 1a, the general process of our power-management design starts from charging serial-connected capacitors using TENG. When the charging operation completes (typically after a half-cycle of TENG operation), the capacitors are disconnected from TENG and connected in parallel for power output. After releasing all the stored energy, the capacitors are serial-connected with TENG again to be charged. The detailed process is illustrated below (as shown in Fig. 1a):

During step I, as the displacement changes from x=0 to x=$x_{max,}$ TENG is connected to a group of capacitors in series, which consists of several (N) identical capacitors with capacitance C, so the extra charges are transferred to the capacitors in series. Usually the external total capacitance $C_E = \frac{C}{N}$ is chosen to be larger than the capacitance of the TENG $C_T(x)$, so that the majority of the maximum short-circuit charge transfer $Q_{SC,\ max}$ can flow into the capacitors. As a result, all the electrodes of these capacitors in series take the same amount of positive or negative charges, as shown in Fig. 1a-I. Providing that the charge amount of up to Q_{L1} is transferred from TENG to the capacitors, the total voltage in the capacitors approaches $\frac{Q_{L1}}{C_E}$. For step II as shown in Fig. 1a-II, once x=$x_{max,}$ these capacitors are disconnected from TENG, and connected in parallel to the external load for power output. Thus, the output charge becomes NQ_{L1} and the voltage is $\frac{Q_{L1}}{NC_E} = \frac{Q_{L1}}{C}$. Meanwhile, the two electrodes of TENG are connected together to achieve the balanced electrostatic status by releasing the residue charges, as the initial status for the next half-cycle. Step III starts from connecting capacitors in series with TENG again. Steps III and IV are similar to steps I and II with transferred charge of Q_{L2}, output voltage of $-\frac{Q_{L2}}{C}$ and output charge of NQ_{L2}, respectively, as shown in Fig. 1a-III and 1a-IV. Hence, through this series-parallel connection conversion of the capacitors, the charge output can be enhanced up to N times, while the voltage is lowered by at least N times.

As stated in Note S1 and Fig. S2, Supplementary information, by using an alternative design it is also possible to utilize the residue charges left in TENG after each half-cycle to output additional energy. However, as N increases, this marginal output energy decreases and approaches zero at N =+∞. So in this paper we only study the design as presented in Fig. 1 that is widely applicable for power-management units with different N.

To quantitatively evaluate the performance of this power-management design for TENG, the built-up V–transferred charge Q plot is utilized to reveal the process and the output energy of each cycle [26]. Here we use the most commonly adopted minimum achievable charge reference state (MACRS) [14,25,26], with (Q, V) status starts from (0, 0) at x=0, as plotted in Fig. 1b. The step I corresponds to the red tilt line from (0, 0) to (Q_{L1}, $\frac{Q_{L1}}{C_E}$), with the slope determined by the external total capacitance C_E. During step II, the two electrodes of TENG are shorted to reset V to be 0, so that the fully charge transfer of $Q_{SC,\ max}$ is achieved, which corresponds to the blue line from (Q_{L1}, $\frac{Q_{L1}}{C_E}$) to ($Q_{SC,\ max}$, 0). Similar to steps I and II but in V < 0 area, the steps III and IV are from ($Q_{SC,\ max}$, 0) to ($Q_{SC,\ max}$−Q_{L2}, $-\frac{Q_{L2}}{C_E}$) and from ($Q_{SC,\ max}$−Q_{L2}, $-\frac{Q_{L2}}{C_E}$) to (0, 0), respectively. Here, we can derive Q_{L1} and Q_{L2} as (see Note S2, Supplementary information, for detailed derivations):

$$Q_{L1} = \frac{C_E Q_{SC,\ max}}{Q_{SC,\ max}/V_{OC,\ max} + C_E} \tag{1a}$$

$$Q_{L2} = \frac{C_E Q_{SC,\ max}}{Q_{SC,\ max}/V'_{max} + C_E} \tag{1b}$$

Please notice that the difference between Q_{L1} and Q_{L2} is only due to the difference between $V_{OC,\ max}$ and V'_{max} which originates from the capacitances of TENG at x=0 and x= x_{max}[26]. For contact-separation (CS) mode [27,28] and lateral-sliding (LS) mode [29–31] TENGs, these two capacitances are different; for single-electrode (SE) mode [32–34] and freestanding-triboelectric-layer (FT) mode [24,25,35] TENGs, the capacitances are the same [26]. To simplify the calculations, we chose sliding FT (SFT) mode TENG with identical capacitances at x=0 and x= x_{max} for calculations and experiments. Therefore, $V_{OC,\ max}$ = $V'_{max,}$ and hence we can use Q_L as it equals to both Q_{L1} and Q_{L2}. Then, the input energy per cycle from TENG to the power-management unit is derived as:

$$E_{in} = 2 \times \frac{1}{2} Q_{SC,\ max} \frac{Q_L}{C_E} = \frac{{Q_{SC,\ max}}^2}{Q_{SC,\ max}/V_{OC,\ max} + C_E} \tag{2}$$

And the output energy from the power-management unit is:

$$E_{out} = 2 \times \frac{1}{2} \frac{{Q_L}^2}{C_E} = \frac{C_E {Q_{SC,\ max}}^2}{(Q_{SC,\ max}/V_{OC,\ max} + C_E)^2} \tag{3}$$

With the increase of C_E, Q_L approaches $Q_{SC,\ max}$, and at the same time the voltage $\frac{Q_L}{C_E}$ decreases, as shown in Fig. 1c. E_{out} can achieve the

Table 1
Definitions of important parameters of a TENG.

Symbol	Definitions
$Q_{SC,\ max}$	The maximum short-circuit transferred charge
$V_{OC,\ max}$	The maximum open-circuit voltage at Q=0
V'_{max}	The maximum achievable absolute voltage at Q=$Q_{SC,\ max}$
E_m	The largest possible energy output per cycle

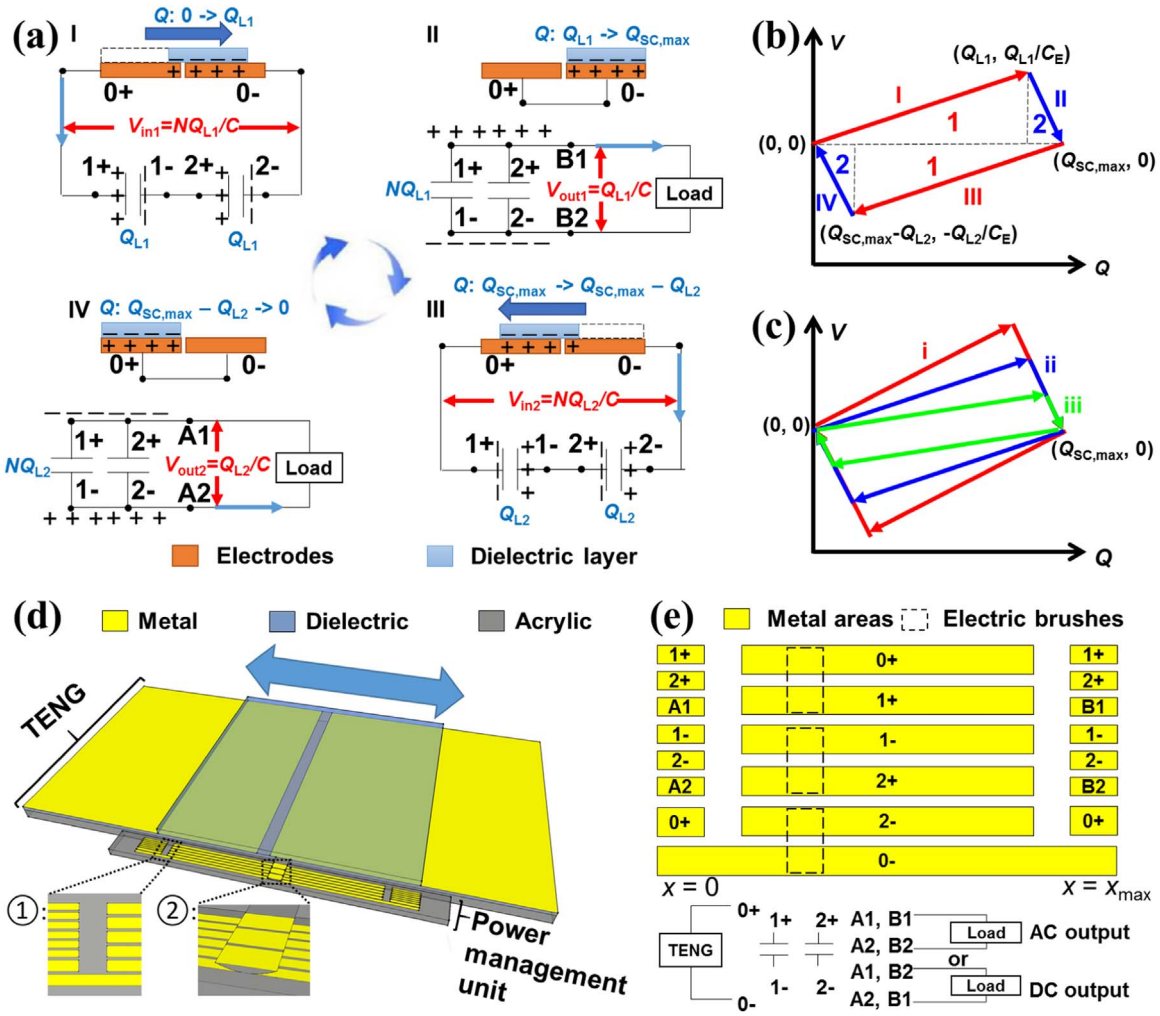

Fig. 1. The auto-power-management design and the motion-triggered unit. (a): the circuit diagram for the four-step power-management, with the charges marked with blue symbols, voltage marked with red symbols, and the nodes marked with black symbols. In these nodes, 0+ and 0− are connected to two electrodes of TENG; 1+/2+ and 1−/2− are connected to two electrodes of capacitors; A1, A2 and B1, B2 are connected to the load; (b): the *V*-*Q* plot of a power-management process showing the four steps; (c): the *V*-*Q* plots with different external total capacitance C_E, for which iii > ii > i; (d): the 3D illustration of the power-management unit. The zoomed-in views for the connection switch area (①, top view) and the electric brushes on top of metal areas (②) are shown in the insets. (e): the design of metal areas in the board and the electric brushes of the motion-triggered power-management unit (top view), with the symbols of nodes corresponding to that in (a).

maximum value when $C_E = \frac{C}{N} = \frac{Q_{SC,\,max}}{V_{OC,\,max}}$[36]:

$$E_{out,\,max} = \frac{Q_{SC,\,max} V_{OC,\,max}}{4} \tag{4}$$

The energy transfer efficiency of this power-management unit is defined as same as previous work [14]:

$$\eta = \frac{E_{out}}{E_m} \tag{5}$$

where E_{out} is the output energy per cycle from power-management unit as defined in Eq. (3), and E_m is the largest possible output energy per cycle for a TENG [26] (Further discussions in Note S3, Supplementary information). Due to Eq. (4), the energy transfer efficiency also reaches the maximum value of 25% when $C_E = \frac{C}{N} = \frac{Q_{SC,\,max}}{V_{OC,\,max}}$:

$$\eta_{max} = \frac{E_{out,\,max}}{E_m} = \frac{\frac{1}{4} Q_{SC,\,max} V_{OC,\,max}}{\frac{1}{2} Q_{SC,\,max} (V_{OC,\,max} + V'_{max})} = 25\% \tag{6}$$

2.2. Design of the motion-triggered power-management unit

As a proof-of-concept demonstration of the new auto-power-management principle, a motion-triggered power-management unit is designed. As a mechanical energy harvester, the operation of TENG is subject to mechanical motions. This motion is able to not only supply the energy source for electricity generation, but also automatically trigger switches for proper operations of the capacitors. Here we design a power-management unit as triggered by motion of the moving part in TENG, based on the principle as described above. An SFT mode TENG is used experimentally. The 3D illustration of a TENG and a power-management unit with N=2 is shown in Fig. 1d. The designed power-management unit includes an acrylic board with metal areas (as called the power-management board) and electric brushes built on the moving part of TENG, with the top view design of the metal areas and the electric brushes as shown in Fig. 1e. The symbols in the metal areas represent the corresponding nodes in Fig. 1a, respectively. In these nodes, 0+ and 0− are the symbols for the two electrodes of the TENG, and the other numbers with + or − are the symbols for two electrodes of each capacitor used. (For example, symbols 1+ and 1− are for electrodes of the 1st capacitor, and so on.) Symbols A1, A2, B1 and B2 are for nodes that are connected to external loads. The areas contacted by the electric brushes are depicted as the dashed frames, and the brushes move between the two extreme positions which are corresponding to x=0 and x=x_{max}, respectively. Thus, when the positions of the brushes are in the middle portion, the middle metal areas

are connected so that the TENG charges the serial-connected capacitors. When the brushes move to the most left-hand or right-hand side, the metal areas in the sides are connected. Thus the capacitors are connected in parallel to output power through A1, A1 or B2, B2, and the two electrodes of TENG are connected to reset the voltage to be 0. Since the polarization of the output current created by each half-cycle from TENG is opposite, A1 and B1, A2 and B2 can be connected, respectively, for the AC output (the AC connection); or A1 and B2, A2 and B1 can be connected, respectively, for the DC output (the DC connection). (Please check Note S4, Supplementary information, for detailed discussions.) The size of the power-management units can be much smaller than TENG as shown in Fig. 1d, and hence the energy loss during friction between electric brushes and the metal areas could be relatively low as compared with the frictional energy loss existing in TENG (< 1%). (Note S5, Supplementary information) The parameters in the power-management unit are also carefully adjusted so that the energy loss while switching the connections is minimum (< 1%). (Note S6 and Fig. S3, Supplementary information) To demonstrate this power-management design, we fabricate the SFT mode TENG with a proof-of-concept power-management unit with N=2, with a picture as shown in Fig. S4a, Supplementary information. The sizes of the power-management units are made to be larger than that in Fig. 1d just for easy fabrication through laser cutting. The power-management unit with N=5 is also fabricated. The parameters and detailed fabrication process are described in the Methods section.

2.3. Setups for experiments

The static part of the TENG and the power-management unit (the electrodes of TENG and the power-management board) are mounted together on a lifting platform, and the moving part of the TENG with a fluorinated ethylene propylene (FEP) film as the dielectric piece and the electric brushes are attached on a linear motor to produce the sliding movement. The relative positions between these parts are carefully adjusted to make sure the electric brushes contact with suitable areas during sliding. The linear motor is usually set with period of ~0.8 s or ~1.2 s and displacement of 45 mm except stated otherwise.

2.4. Output measurements of TENG only

The output performance of TENG without any power-management unit is firstly measured. The maximum short-circuit charge transfer $Q_{SC,\ max}$ and the maximum open-circuit voltage $V_{OC,\ max}$ of TENG are measured to be 161 nC (Fig. 2a) and 470 V (Fig. S4b, Supplementary information), respectively. The short-circuit current can achieve ~1 μA, as shown in Fig. S4c, Supplementary information. Under the triggering period of 1 s, the average power output while directly connecting TENG to external load resistance is plotted in Fig. S4d, Supplementary information, with the optimized average power of 30.31 μW.

2.5. Output of TENG with power-management unit of N=2

The V-Q plots of the TENG connected to the power-management unit of N=2 with various capacitances C of 1 nF, 11.6 nF or 105 nF, respectively, are displayed in Fig. 2b. The measurement circuit is shown in Fig. S5a, Supplementary information. The shapes of the V-Q plots are very consistent with that derived theoretically in Fig. 1b and c. The zoomed-in V-Q plot of C=105 nF is shown as Fig. S5b, Supplementary information. Through the AC connection, the periodically oscillated short-circuit output charge transfers $Q_{SC,\ out}$ and open-circuit output voltages $V_{OC,\ out}$ are measured in Fig. 2c and d. The $V_{OC,\ out}$ are measured in the steady states as stated in Note S7, Supplementary information. Here we confirm that with the higher capacitance C used, the higher $Q_{SC,\ out}$ and the lower $V_{OC,\ out}$ can be achieved. The $Q_{SC,\ out}$ is up to 320 nC, which is about twice of $Q_{SC,\ max}$. Through the DC connection, both the charge transfers and the current can be directly rectified to be unidirectional (Fig. 2e and f). The high output current peaks in both the AC (Fig. S5c, Supplementary information) and DC connections mainly originate from instantaneous release of charges from capacitors [37]. (Note S8, Supplementary information).

2.6. Output of TENG with power-management unit of N=5

The design of the metal areas and the electric brushes in the power-management unit with N=5 is presented in Fig. 3a (top view), where nodes 0+ and 0− are for two electrodes of TENG, nodes A1, A2, B1 and B2 are connected to the load, and other nodes are connected to 5 capacitors, respectively. The photo of the fabricated power-management board is shown in Fig. S6a, Supplementary information. The measured V-Q plots with different capacitances of each capacitor C of 5.8 nF, 11.6 nF or 100 nF, respectively, are depicted in Fig. 3b, which are consistent with theoretical derivations. With the AC connection, high short-circuit output charge $Q_{SC,\ out}$ up to ~800 nC is obtained, as shown in Fig. S6b, Supplementary information, and the open-circuit voltages $V_{OC,\ out}$ are shown in Fig. S6c, Supplementary information. With the DC connection, this charge transfers become unidirectional (Fig. 3c), which can be demonstrated to charge a supercapacitor of C_S=5 mF with a charging rate of about 5 times as that without power-management unit (through a conventional full-wave bridge rectifier) (Fig. 3d). After 250 s of charging, the TENG with power-management unit charges the supercapacitor to be V_1=98.85 mV while the charging rate is R_1=0.28 mV/s; for the TENG without power-management unit, the voltage and the charing rate achieved are V_2=20.52 mV and R_2=0.069 mV/s, respectively. At this time, the enhancement of the energy transfer efficiency brought by the power-management unit can be estimated at about 19.64 times through the following equation:

$$\frac{\eta_1}{\eta_2} = \frac{P_1}{P_2} = \frac{V_1(R_1C_S)}{V_2(R_2C_S)} = \frac{V_1R_1}{V_2R_2} \tag{7}$$

in which η_1 and η_2 are the energy efficiencies with and without the power-management unit, while P_1 and P_2 are the average power outputs with and without the power-management unit, respectively.

2.7. The energy efficiency

For the power-management units with N=2 and N=5, 6 sets of experimental data are acquired with different C_E. For each C_E, E_{out} is calculated by:

$$E_{out} = 2\cdot\frac{1}{2}\frac{Q_{SC,out}{}^2}{NC} = \frac{Q_{SC,out}{}^2}{NC} \tag{8}$$

These experimental E_{out} are plotted as dots in Fig. 3e, which are consistent with that calculated by Eq. (3), as shown as the line in Fig. 3e. The highest E_{out} during our experiments is 1.74 μJ, and the corresponding experimental maximum energy transfer efficiency (from Eq. (5)) is 23.0%. As stated in Note S9, Supplementary information, this energy transfer efficiency is equivalent to 57.3% by using another definition of the energy transfer efficiency as reported by Niu et al., which is comparable to that of the previous work [12].

2.8. Expand the system for broader applications

This design of the power-management unit can be expanded to different modes of TENG. As illustrated in Fig. 4a, the contact-separation (CS) mode TENG, that can harvest body motion and vibration energies [38–40], is also able to be integrated with the power-management unit vertically. A CS mode TENG is fabricated, with the maximum short-circuit charge transfer measured as about 75 nC (Fig. S7a, Supplementary information). With a fabricated power-management unit (N=2), similar V-Q plots are measured as predicted

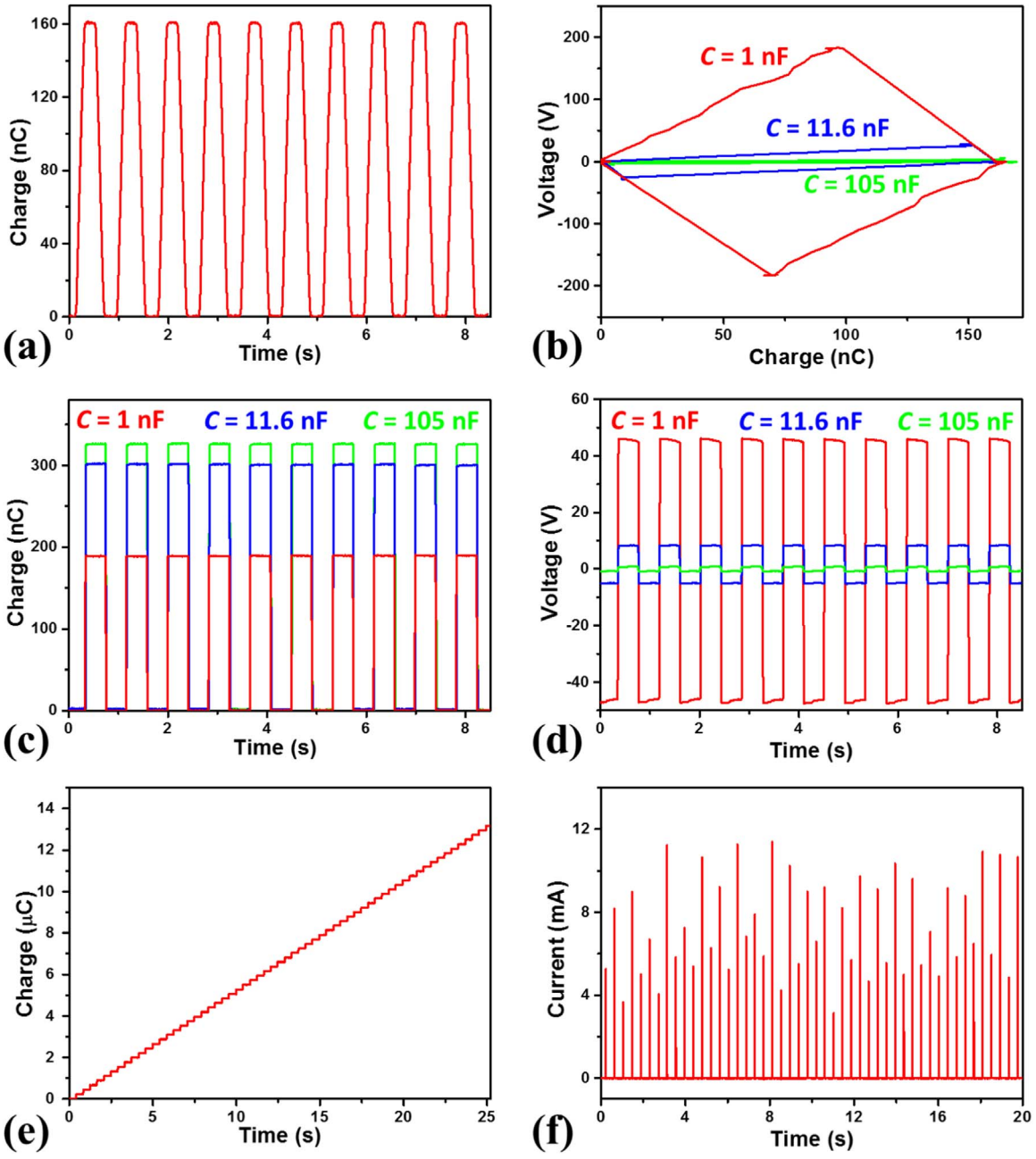

Fig. 2. Output performance of TENG through the power-management unit with N=2. (a): the short-circuit charge transfers of TENG without any power-management unit; (b): the V-Q plots of TENG through the power-management unit with various capacitances; (c) and (d): the short-circuit output charge transfers and open-circuit output voltages through AC connection; (e) and (f): the short-circuit output charge transfer and peak current through DC connection (each capacitor C=1 nF). The triggering period is ~0.8 s.

(Fig. 4b), and $Q_{SC,\ out}$ of nearly 150 nC are measured for both the AC and DC connections (Fig. S7 b and c, Supplementary information). As a result of the varied capacitance of TENG in contact and separation, there is a little difference between $Q_{SC,\ out}$ in the first-half and the second-half cycle due to different Q_{L1} and Q_{L2}, as consistent with the discussions above. Besides, as shown in Fig. 4c, this design also perfectly fits the rotational TENG which is the most powerful TENG design so far for harvesting wind and ocean energies [13,41], since the rotational power-management unit can be easily integrated inside TENG with an extremely small size. By integration of the power-management unit in different modes of TENGs, it is possible to improve the energy transfer efficiency while utilizing mechanical energy harvested towards various applications.

For practical applications which usually require a stable DC power, the power-management unit can be connected to a suitable energy storage unit (a battery or a supercapacitor) to stabilize the voltage supply [42–44]. Through that, TENG, the power-management unit, the energy storage unit and the load build a self-powered system. Optimization of the total efficiency of the whole self-powered system is worth to be further investigated towards practical applications.

3. Discussions

Our motion-triggered power-management unit demonstrates the new auto-power-management principle based on connection switches between capacitors. Please notice that the motion-triggered unit is just a proof-of-concept approach to achieve the principle. The switches of the connections could also be realized by other designs. In this new principle, the number of capacitors (N) determines the largest level of the enhancement in the output charge, and the capacitance of each

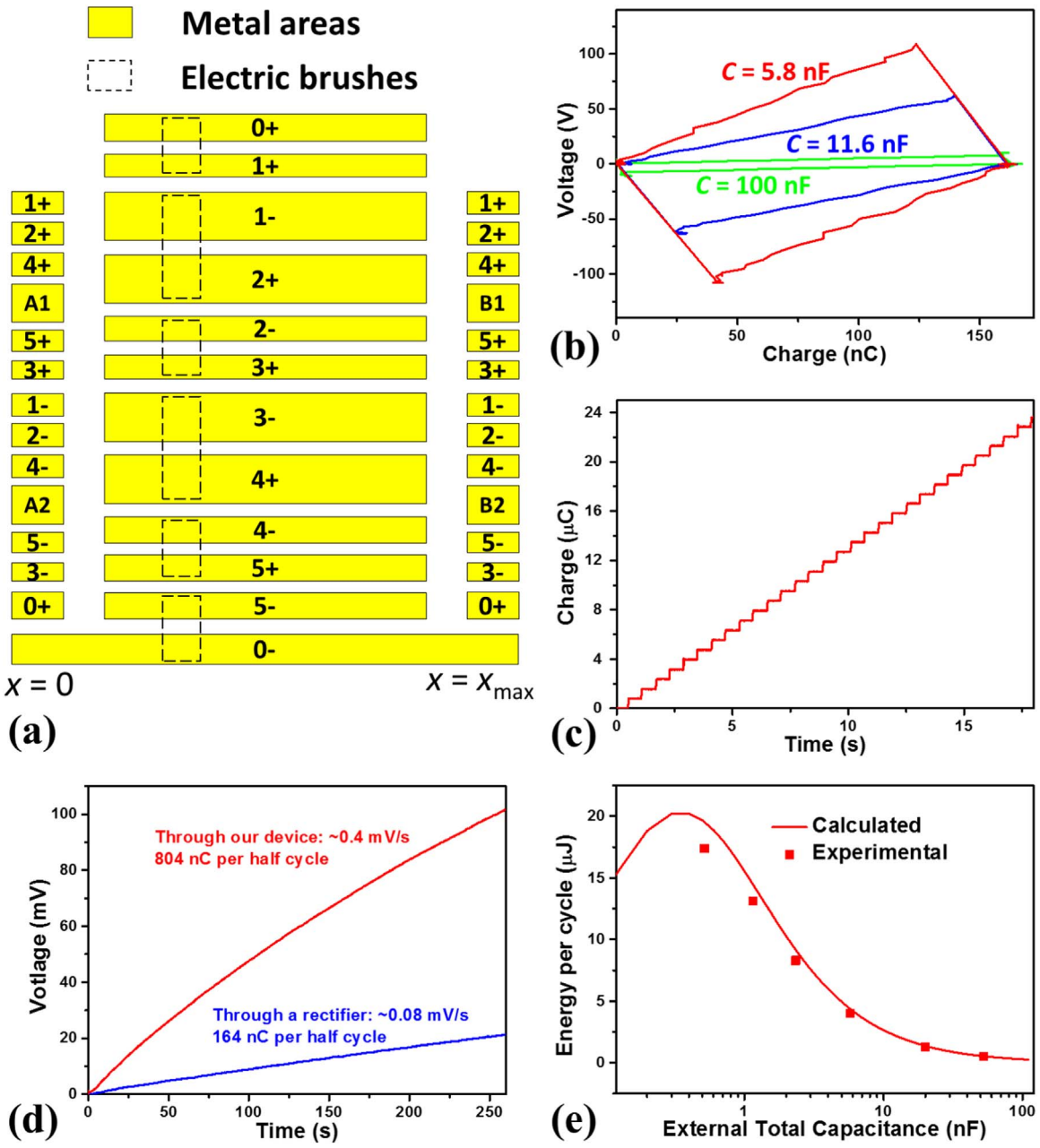

Fig. 3. The output performance of power-management unit with N=5. (a): the design of the power-management board and the electric brushes (top view). (b): the V-Q plots of TENG using the power-management unit with various capacitors; (c) and (d): the short-circuit charge transfer and the charging plot of a 5 mF supercapacitor through the DC connection (each capacitor C=100 nF); (e): the experimental and calculated (by Eq. (3)) total output energy per cycle. The triggering period is ~1.2 s except the one during charging the supercapacitor in (e) which is~0.8 s.

capacitor (C) along with the number of capacitors (N) determines the final output impedance (as stated in Note S10 and Fig. S8 a~b, Supplementary information). This principle makes itself a unique power-management solution with its own characteristics as discussed below:

Firstly, it is possible to utilize this power-management principle to harvest low-frequency low-power-level mechanical energy, which cannot be achieved by other power-management units based on the electromagnetic effect. As the core part for other power management systems, coupled inductors [12] or transformers [18] may consume a large quantity of power. To operate these units properly, a certain power of at least ~100 μW level is required, and usually the power outputs of TENGs used in their studies are in ~mW level [9,12,17,18]. To achieve this large power output, either large volume of TENG or a certain large triggering frequency level is required. Based on our new principle, since charge transfers between capacitors are always almost instantaneous (Note S11, Supplementary information), there is no such a threshold power/frequency required for its operation so that even the harvested energy in minimal scale and extremely low frequency can be effectively managed and utilized (Fig. S8c, Supplementary information). This feature enables the possibility to utilize varieties of mechanical energy delivered by TENG, especially that with low frequency and low power level. The maximum frequency of the power-management design mainly depends on that of the TENG. This kind of power-management solution is demanded by TENG that is mainly targeted at low-frequency small-scale energy harvesting [19].

Secondly, without inductors and iron cores, it is much easier for systems based on our power-management principle towards scaled-down fabrication in microscale, which can be easily implemented by well-developed technologies such as printed circuit board (PCB) and

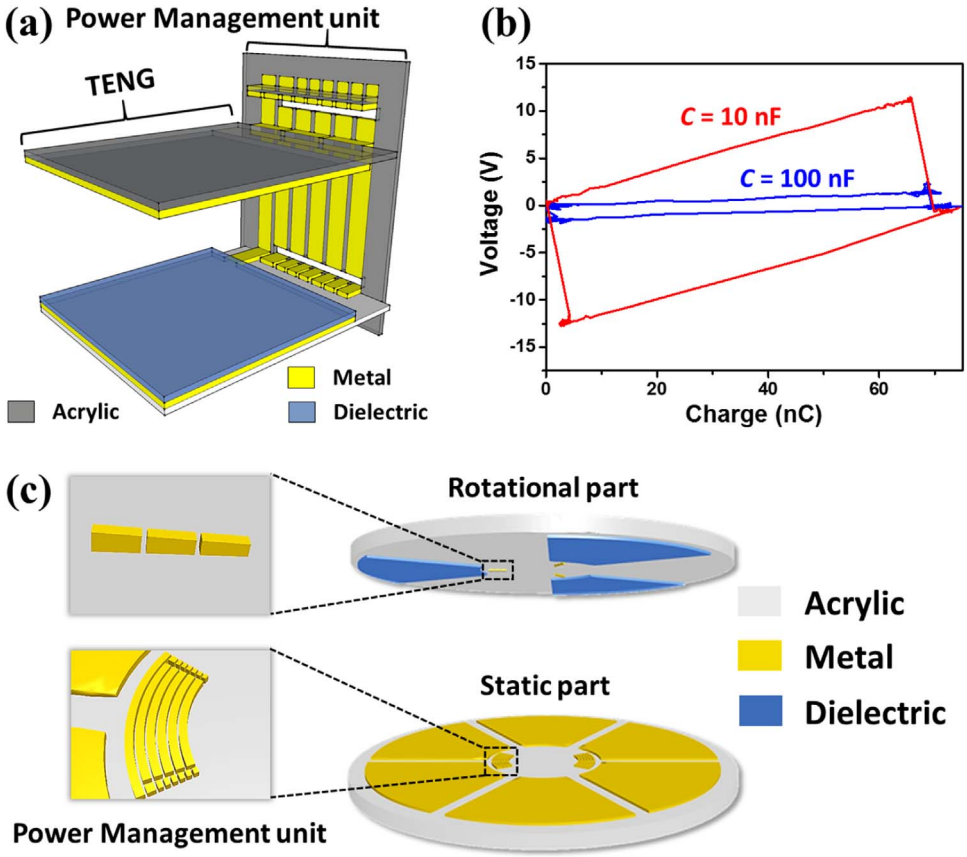

Fig. 4. Expansion of the system towards multiple applications and operation modes. (a) and (b): the 3D illustration and *V-Q* plots of the power-management unit for CS mode TENG; (c): the 3D illustration of the power-management unit (built inside the TENG) for rotational SFT mode TENG. The insets show zoomed-in pictures of the electric brushes (upper) and the metal areas (lower). The triggering period for the CS mode TENG is ~12.9 s.

optical lithography.

At the last but not least, compared to previous systems with coupled inductors or transformers which are heavy and bulky, our power-management unit could be light in weight, small in size and well integrated with TENG already. They can be packed as a low-voltage but high-current power cell, which is portable and scalable for effectively utilizing ambient mechanical energy. Based on the same working principle, it is also possible to make power-management units flexible and wearable, if logic control circuits with low power consumptions [12] are introduced to control the connection switches of the capacitors.

4. Conclusions

In summary, a novel power-management principle based on automatic connection switches of capacitors is designed for TENG. This principle is firstly theoretically analyzed, and then proof-of-concept power-management units as automatically triggered by the motion of TENG are fabricated and experimentally characterized, to achieve the lowered voltage but greatly improved charge outputs with the energy transfer efficiency comparable to the previous work. This power-management unit can be extended to accommodate multiple modes of TENG for various applications. This power-management design shows plenty of advantages such as capability for managing low-frequency small-scale power, high scalability and light weight, which makes a revolutionary step towards TENG-based self-powered systems.

5. Experimental section

5.1. Fabrication of SFT mode TENG

Typically, an acrylic sheet (thickness of 3 mm) was cut into 5 cm×10 cm by laser cutter as the substrate. Then two electrodes made by copper (Cu) or gold (Au) were deposited on a FEP film (50 μm in thickness) with an interval gap of 2 mm by physical vapor deposition (PVD 75). Finally, the FEP film was adhered onto the acrylic sheet with the electrodes facing up to form the electricity generation part of TENG.

The moving part of the TENG was attached with the electric brushes, as fabricated on an acrylic sheet (6 mm in thickness) composed by a 4.5 cm×3 cm area on one end (short-wide end) and a 5.2 cm×1 cm area for N=2 or 10 cm×1 cm area for N=5 on the other end (long-narrow end). The moving part of TENG was fabricated by sticking a 4.5 cm×3 cm FEP film onto the short-wide end, and then several pieces of metal foils (usually steel, copper or titanium, each with 6–12 mm in width) were bent and adhered on the long-narrow end as the electric brushes, with use of kapton tapes to fix them. The sizes and positions of the brushes were adjusted to match the designed metal areas in the power-management board.

5.2. Fabrication of CS mode TENG

An acrylic sheet (thickness of 3 mm) was cut into two 5 cm×5 cm pieces by laser cutter as the substrate. Then two 4.5 cm×4.5 cm pieces of FEP films (50 μm in thickness) are deposited with Cu by physical vapor deposition (PVD 75). Finally, the FEP films was adhered onto the acrylic sheets with Cu side of one piece facing to the FEP side of the other piece to form a CS mode TENG. The top acrylic sheet with the Cu

side facing out is attached with steel strips on the side as the electric brushes. The power-management board is fabricated by the method as described below and attached to the bottom acrylic sheet perpendicularly.

5.3. Fabrication of the power-management board

The fabrication of the board with N=2 is described as an example. In the beginning, an acrylic sheet (thickness of 3 mm) was cut by a laser cutter into 4.6 cm×7.2 cm as the substrate. The Cu or Au metal were deposited on the front side of the board by PVD 75 to form the metal areas, with the mask made by other acrylic sheets cut by the laser cutter. Six grooves were cut on the back side of the substrate so that the Cu wires can be arranged on the back of the board. Then several Cu wires were arranged on the backside of the as-fabricated board. The electrodes with the same marks were connected together by these Cu wires, respectively, and the TENG and capacitors were connected to 0+ and 0−, 1+ and 1−, 2+ and 2−, and *etc*, respectively. The board with N=5 and the board for CS mode TENG were prepared with the similar procedures but with different sizes and positions of the metal areas.

5.4. Electrical measurement and motion control

The output voltage signals, charge transfers and current signals of the device were acquired *via* the Keithley 6514 System Electrometers. The *V-Q* plots were measured by two electrometers at the same time as shown in Fig. S5a, Supplementary information. The linear slide motion was produced by a linear motor (T - Profile Rail Guides).

Acknowledgements

Dr. Y. Zi, H. Guo and Dr. J. Wang contributed equally to this work. This research was supported by the Hightower Chair foundation and the 'thousands talents' program for pioneer researcher and his innovation team, China.

Appendix A. Supporting information

Supplementary data associated with this article can be found in the online version at doi:10.1016/j.nanoen.2016.11.025.

References

[1] Z.L. Wang, J. Song, Piezoelectric nanogenerators based on zinc oxide nanowire arrays, Science 312 (5771) (2006) 242–246.
[2] R. Hinchet, S.-W. Kim, Wearable and implantable mechanical energy harvesters for self-powered biomedical systems, ACS Nano 9 (8) (2015) 7742–7745.
[3] C. Dagdeviren, B.D. Yang, Y. Su, P.L. Tran, P. Joe, E. Anderson, J. Xia, V. Doraiswamy, B. Dehdashti, X. Feng, B. Lu, R. Poston, Z. Khalpey, R. Ghaffari, Y. Huang, M.J. Slepian, J.A. Rogers, Conformal piezoelectric energy harvesting and storage from motions of the heart, lung, and diaphragm, Proc. Natl. Acad. Sci. 111 (5) (2014) 1927–1932.
[4] S. Park, H. Kim, M. Vosgueritchian, S. Cheon, H. Kim, J.H. Koo, T.R. Kim, S. Lee, G. Schwartz, H. Chang, Z. Bao, Stretchable energy-harvesting tactile electronic skin capable of differentiating multiple mechanical stimuli modes, Adv. Mater. 26 (43) (2014) 7324–7332.
[5] F.-R. Fan, Z.-Q. Tian, Z.L. Wang, Flexible triboelectric generator, Nano Energy 1 (2) (2012) 328–334.
[6] Z.L. Wang, Triboelectric nanogenerators as new energy technology for self-powered systems and as active mechanical and chemical sensors, ACS Nano 7 (11) (2013) 9533–9557.
[7] Z.L. Wang, Triboelectric nanogenerators as new energy technology and self-powered sensors - Principles, problems and perspectives, in *Faraday Discussions*, The Royal Society of Chemistry, 2014.
[8] H. Guo, Q. Leng, X. He, M. Wang, J. Chen, C. Hu, Y. Xi, A. Triboelectric, Generator based on checker-like interdigital electrodes with a sandwiched pet thin film for harvesting sliding energy in all directions, Adv. Energy Mater. 5 (1) (2015) n/a-n/a.
[9] H. Guo, X. He, J. Zhong, Q. Zhong, Q. Leng, C. Hu, J. Chen, L. Tian, Y. Xi, J. Zhou, A nanogenerator for harvesting airflow energy and light energy, J. Mater. Chem. A 2 (7) (2014) 2079–2087.
[10] J. Bae, J. Lee, S. Kim, J. Ha, B.-S. Lee, Y. Park, C. Choong, J.-B. Kim, Z.L. Wang, H.-Y. Kim, J.-J. Park, U.I. Chung, Flutter-driven triboelectrification for harvesting wind energy, Nat. Commun. 5 (2014) 4929.
[11] Y. Yu, Z. Li, Y. Wang, S. Gong, X. Wang, Sequential infiltration synthesis of doped polymer films with tunable electrical properties for efficient triboelectric nanogenerator development, Adv. Mater. 27 (33) (2015) 4938–4944.
[12] S. Niu, X. Wang, F. Yi, Y.S. Zhou, Z.L. Wang, A universal self-charging system driven by random biomechanical energy for sustainable operation of mobile electronics, Nat. Commun. 6 (2015) 8975.
[13] H. Guo, Z. Wen, Y. Zi, M.-h. Yeh, J. Wang, L. Zhu, C. Hu, Z.L. Wang, A water-proof triboelectric-electromagnetic hybrid generator for energy harvesting in harsh environments, Adv. Energy Mater. 6 (6) (2016).
[14] Y. Zi, J. Wang, S. Wang, S. Li, Z. Wen, H. Guo, Z.L. Wang, Effective energy storage from a triboelectric nanogenerator, Nat. Commun. 7 (2016) 10987.
[15] X. Pu, M. Liu, L. Li, C. Zhang, Y. Pang, C. Jiang, L. Shao, W. Hu, Z.L. Wang, Efficient charging of Li-ion batteries with pulsed output current of triboelectric nanogenerators, Adv. Sci. (2015) n/a-n/a.
[16] K. Zhang, X. Wang, Y. Yang, Z.L. Wang, Hybridized electromagnetic–triboelectric nanogenerator for scavenging biomechanical energy for sustainably powering wearable electronics, ACS Nano 9 (4) (2015) 3521–3529.
[17] X. Zhong, Y. Yang, X. Wang, Z.L. Wang, Rotating-disk-based hybridized electromagnetic-triboelectric nanogenerator for scavenging biomechanical energy as a mobile power source, Nano Energy 13 (2015) 771–780.
[18] L.-C. Luo, D.-C. Bao, W.-Q. Yu, Z.-H. Zhang, T.-L. Ren, A low input current and wide conversion ratio buck regulator with 75% efficiency for high-voltage triboelectric nanogenerators, Sci. Rep. 6 (2016) 19246.
[19] Y. Zi, H. Guo, Z. Wen, M.-H. Yeh, C. Hu, Z.L. Wang, Harvesting low-frequency (< 5 Hz) irregular mechanical energy – A possible killer application of triboelectric nanogenerator, ACS Nano 10 (4) (2016) 4797–4805.
[20] A. Cabrini, L. Gobbi, G. Torelli, Voltage gain analysis of integrated fibonacci-like charge pumps for low power applications, I*EEE* Trans. Circuits Syst. II: Express Briefs 54 (11) (2007) 929–933.
[21] J.A. Starzyk, J. Ying-Wei, Q. Fengjing, A DC-DC charge pump design based on voltage doublers, IEEE Trans. Circuits Syst. I: Fundam. Theory Appl. 48 (3) (2001) 350–359.
[22] C.-M. Kyung, Nano Devices and Circuit Techniques for Low-energy Applications and Energy Harvesting, Springer, 2016.
[23] C.M.F. Carvalho, N.F.S.V. Paulino, CMOS indoor light energy harvesting system for wireless sensing applications, Springer, 2016.
[24] S. Wang, Y. Xie, S. Niu, L. Lin, Z.L. Wang, Freestanding triboelectric-layer-based nanogenerators for harvesting energy from a moving object or human motion in contact and non-contact modes, Adv. Mater. 26 (18) (2014) 2818–2824.
[25] S. Niu, Y. Liu, X. Chen, S. Wang, Y.S. Zhou, L. Lin, Y. Xie, Z.L. Wang, Theory of freestanding triboelectric-layer-based nanogenerators, Nano Energy 12 (2015) 760–774.
[26] Y. Zi, S. Niu, J. Wang, Z. Wen, W. Tang, Z.L. Wang, Standards and figure-of-merits for quantifying the performance of triboelectric nanogenerators, Nat. Commun. 6 (2015) 8376.
[27] S. Niu, S. Wang, L. Lin, Y. Liu, Y.S. Zhou, Y. Hu, Z.L. Wang, Theoretical study of contact-mode triboelectric nanogenerators as an effective power source, Energy Environ. Sci. 6 (12) (2013) 3576–3583.
[28] G. Zhu, C. Pan, W. Guo, C.-Y. Chen, Y. Zhou, R. Yu, Z.L. Wang, Triboelectric-generator-driven pulse electrodeposition for micropatterning, Nano Lett. 12 (9) (2012) 4960–4965.
[29] S. Niu, Y. Liu, S. Wang, L. Lin, Y.S. Zhou, Y. Hu, Z.L. Wang, Theory of sliding-mode triboelectric nanogenerators, Adv. Mater. 25 (43) (2013) 6184–6193.
[30] S. Wang, L. Lin, Y. Xie, Q. Jing, S. Niu, Z.L. Wang, Sliding-triboelectric nanogenerators based on in-plane charge-separation mechanism, Nano Lett. 13 (5) (2013) 2226–2233.
[31] G. Zhu, J. Chen, Y. Liu, P. Bai, Y.S. Zhou, Q. Jing, C. Pan, Z.L. Wang, Linear-grating triboelectric generator based on sliding electrification, Nano Lett. 13 (5) (2013) 2282–2289.
[32] S. Niu, Y. Liu, S. Wang, L. Lin, Y.S. Zhou, Y. Hu, Z.L. Wang, Theoretical investigation and structural optimization of single-electrode triboelectric nanogenerators, Adv. Funct. Mater. 24 (22) (2014) 3332–3340.
[33] Y. Yang, H. Zhang, J. Chen, Q. Jing, Y.S. Zhou, X. Wen, Z.L. Wang, Single-electrode-based sliding triboelectric nanogenerator for self-powered displacement vector sensor system, ACS Nano 7 (8) (2013) 7342–7351.
[34] Y. Yang, Y.S. Zhou, H. Zhang, Y. Liu, S. Lee, Z.L. Wang, A single-electrode based triboelectric nanogenerator as self-powered tracking system, Adv. Mater. 25 (45) (2013) 6594–6601.
[35] S. Wang, S. Niu, J. Yang, L. Lin, Z.L. Wang, Quantitative measurements of vibration amplitude using a contact-mode freestanding triboelectric nanogenerator, ACS Nano 8 (12) (2014) 12004–12013.
[36] S. Niu, Y. Liu, Y.S. Zhou, S. Wang, L. Lin, Z.L. Wang, Optimization of triboelectric nanogenerator charging systems for efficient energy harvesting and storage, Electron Devices IEEE Trans. 62 (2) (2015) 641–647.
[37] G. Cheng, Z.-H. Lin, L. Lin, Z.-l. Du, Z.L. Wang, Pulsed nanogenerator with huge instantaneous output power density, ACS Nano 7 (8) (2013) 7383–7391.
[38] J. Chen, G. Zhu, W. Yang, Q. Jing, P. Bai, Y. Yang, T.-C. Hou, Z.L. Wang, Harmonic-resonator-based triboelectric nanogenerator as a sustainable power source and a self-powered active vibration sensor, Adv. Mater. 25 (42) (2013) 6094–6099.
[39] J. Yang, J. Chen, Y. Yang, H. Zhang, W. Yang, P. Bai, Y. Su, Z.L. Wang, Broadband vibrational energy harvesting based on a triboelectric nanogenerator, Adv. Energy Mater. 4 (6) (2014) n/a-n/a.
[40] W. Yang, J. Chen, G. Zhu, J. Yang, P. Bai, Y. Su, Q. Jing, X. Cao, Z.L. Wang, Harvesting energy from the natural vibration of human walking, ACS Nano 7 (12) (2013) 11317–11324.

[41] G. Zhu, J. Chen, T. Zhang, Q. Jing, Z.L. Wang, Radial-arrayed rotary electrification for high performance triboelectric generator, Nat. Commun. 5 (2014) 3426.
[42] S. Wang, Z.-H. Lin, S. Niu, L. Lin, Y. Xie, K.C. Pradel, Z.L. Wang, Motion charged battery as sustainable flexible-power-unit, ACS Nano 7 (12) (2013) 11263–11271.
[43] J. Wang, X. Li, Y. Zi, S. Wang, Z. Li, L. Zheng, F. Yi, S. Li, Z.L. Wang, A flexible fiber-based supercapacitor–triboelectric-nanogenerator power system for wearable electronics, Adv. Mater. 27 (33) (2015) 4830–4836.
[44] J. Wang, Z. Wen, Y. Zi, P. Zhou, J. Lin, H. Guo, Y. Xu, Z.L. Wang, All-plastic-materials based self-charging power system composed of triboelectric nanogenerators and supercapacitors, Adv. Funct. Mater. 26 (7) (2016) 1070–1076.